Rev. Adv. Mater. Sci. 54 (2018) 93-105

PHASE TRANSFORMATIONS «AMORPHIZATION ⇔ CRYSTALLIZATION» IN METALLIC MATERIALS INDUCED BY SEVERE PLASTIC DEFORMATION

A.M. Glezer[1,2], R.V. Sundeev[3] and A.V. Shalimova[2]

[1]National University of Science and Technology "MISIS", Moscow, Russia
[2]I.P.Bardin Central Research Institute for Ferrous Metallurgy, Moscow, Russia
[3]MIREA - Russian Technological University, Moscow, Russia

Received: June 22, 2018

Abstract. In this review we are considered systematically the phenomenon of deformation-induced phase transformations from crystalline intermetallic compounds and complex phases to amorphous state and vice versa phase transformations from amorphous state to crystalline one upon severe plastic deformation at different temperatures. The nature and structural features of these transitions essentially for high pressure torsion deformation are analyzed in the frame of basic principles of nonequilibrium thermodynamics. The effects of phase cycling and a stationary amorphous – nanocrystalline state formation at significant deformations is discussed in details.

1. INTRODUCTION

Systematic studies of structural regularities typical to metallic materials in the process of severe plastic deformation (SPD) are actively continuing [1]. In particular, many interesting and important results were obtained on samples subjected to high pressure torsion (HPT) [2]. The monograph [3] formulated the physical principles underlying the SPD method, and established the characteristic features inherent in this type of deformation. The most significant among them is the experimentally proved phenomenon of the phase transition of some crystalline solid solutions and intermetallic compounds to the amorphous state and, conversely, the transformation of the initially amorphous state of the alloys to a crystalline state under the influence of SPD [4,5]. At first glance, apparently contradictory results were obtained. On the one hand, HPT of amorphous alloys leads to their partial transition to a crystalline (more precisely, nanocrystalline) state. On the other hand, HPT of the same partially crystallized alloys can lead to dissolution of the crystalline phase, that is, a tendency to return to the original amorphous state is observed. The observed contradiction is illusory and can be logically explained taking into account the specific structural processes occurring at SPD, within the framework of nonequilibrium thermodynamics [6].

2. DEFORMATION-INDUCED AMORPHIZATION

The most interesting task, in our opinion, is to reveal of the structural mechanism of the phase transition during SPD from the crystalline state to the amorphous one. The structural and thermodynamic aspects of the deformation-induced amorphization under SPD are the subject of vivid discussion [7-11]. The most illustrative example is titanium nickelide TiNi, for which the transition to the amorphous state is fixed after HPT in the Bridgman chamber [12-14] and after cold rolling [15]. It can be assumed that a crystal containing a very high con-

Corresponding author: R.V. Sundeev, e-mail: sundeev55@yandex.ru

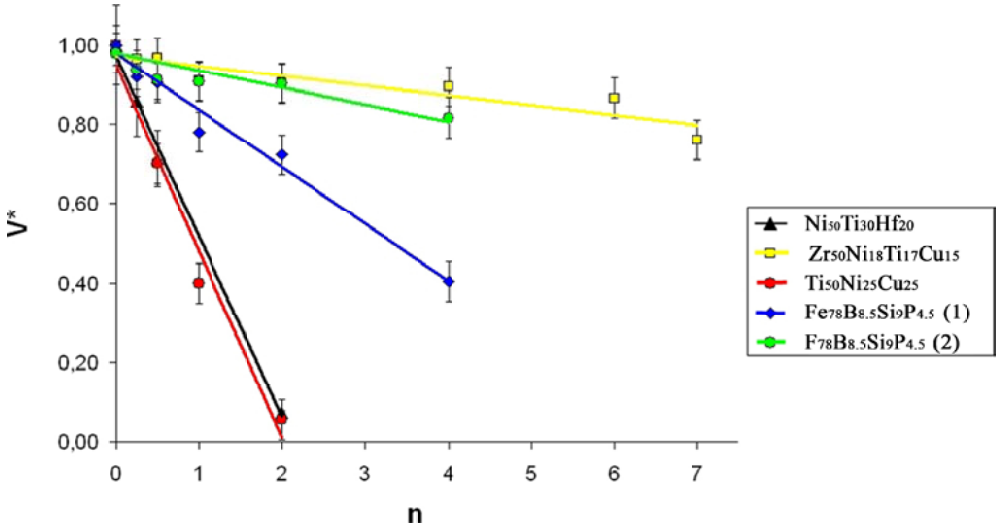

Fig. 1. Dependence of the change in the reduced volume fraction of the crystalline phase *V** for the investigated alloys on the value of *n*.

centration of linear and point defects appears under the conditions of SPD to be thermodynamically unstable to transition to an amorphous state, especially if the difference between the values of the free energies of the crystalline and amorphous states is small. As a rule, this process develops in multicomponent metal systems prone to amorphization (mainly based on Pd-Cu, Ti-Zr, Zr-Cu, Mg-Cu, TiNi-TiCu) [3].

The main regularities of amorphization in the HPT process of the crystalline multicomponent $Ni_{50}Ti_{30}Hf_{20}$, $Ti_{50}Ni_{25}Cu_{25}$, and $Zr_{50}Ni_{18}Ti_{17}Cu_{15}$ alloys in the initially single-phase state and $Fe_{78}B_{8.5}Si_9P_{4.5}$ alloy both in the initially single-phase (1) and initially diphasic (2) states were studied in [16]. For all the alloys studied, the change in the fraction of the crystalline phase (*V*) was definitely determined with increasing deformation (an increase in the number of revolutions *n*) and a dependence *V*(n)* was constructed (Fig. 1). The values of the volume fraction in Fig. 1 were normalized to 100% of the original crystalline phase at $n = 0$ *(V*)*.

The slope of the dependences *V*(n)* characterizes the value of the propensity to deformation-induced amorphization $\kappa_c = |dV^*/dn|$. The numerical values of κ_c and κ_p (for individual phases) in the studied single-phase and two-phase alloys, respectively, are given in Table 1.

In accordance with the data in the table and Fig. 1 it can be seen that all the studied alloys can be conditionally divided into two groups:

• alloys with a high value of κ_c (the first group) - alloys $Ni_{50}Ti_{30}Hf_{20}$, $Ti_{50}Ni_{25}Cu_{25}$ and $Fe_{78}B_{8.5}Si_9P_{4.5}$ (1) in a single-phase state;

• alloys with a low value of κ_c (the second group) - alloys $Zr_{50}Ni_{18}Ti_{17}Cu_{15}$ and $Fe_{78}B_{8.5}Si_9P_{4.5}$ (2) in the two-phase state.

The main factors determining the tendency of crystalline alloys and individual crystalline phases to deformation-induced amorphization in the process of torsion under high pressure were revealed [16]. It is shown that the transformation of the "crystal-amorphous state" is determined by: the propensity to accumulate deformation defects in a crystal

Table 1. The values of κ_c and κ_p for the studied alloys.

Alloy	κ_c	Phase composition	κ_p
$Ti_{50}Ni_{25}Cu_{25}$	45.5	A19	45.5
$Ni_{50}Ti_{30}Hf_{20}$	45.5	B19'	45.5
$Zr_{50}Ni_{18}Ti_{17}Cu_{15}$	2.5	Zr_2Ni	2.0
		Zr-Ti (Ni,Cu)	0.5
$Fe_{78}B_{8.5}Si_9P_{4.5}$ (1)	13.7	α-phase	13.7
$Fe_{78}B_{8.5}Si_9P_{4.5}$ (2)	3.6	$Fe_3(B,P)$	3.5
		α-(Fe-Si)	0.1

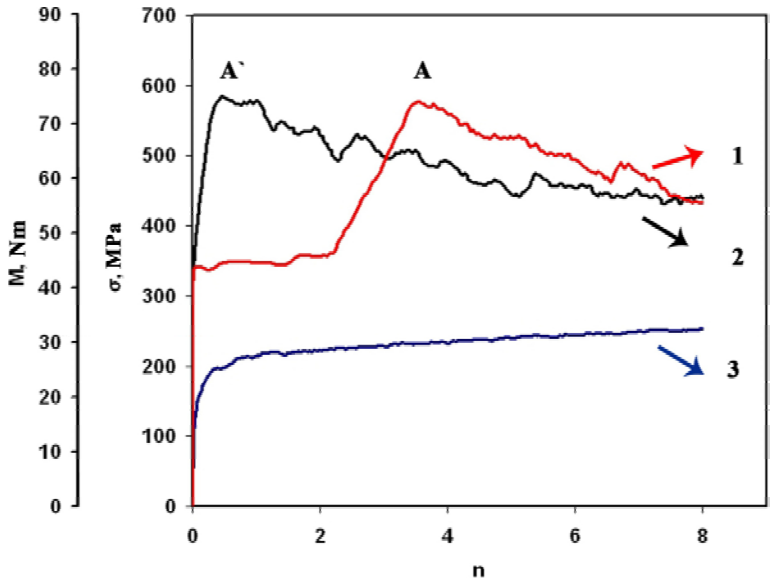

Fig. 2. Dependence of *Ì(n)* and s*(n)* during HPT at 293K: 1 - initial crystalline $Ti_{50}Ni_{25}Cu_{25}$ alloy, 2 - initially amorphous $Ti_{50}Ni_{25}Cu_{25}$ alloy, 3 - crystalline copper.

under mechanical action, the thermodynamic stability of the crystalline phases included in the composition of the alloy, and the possibility of the diffusion processes necessary for changing the chemical composition of the crystalline and amorphous phases in the process deformation. The effect of deformation-induced amorphization of multicomponent crystalline alloys is determined by the additive propensity to deformation-induced amorphization of crystalline phases included in the composition of alloys. It was found that the propensity for deformation-induced amorphization in torsion under high pressure conditions at room temperature differs significantly from the tendency toward amorphization during quenching from the liquid state [17]. It is assumed that this is due to the difference in physical parameters controlling amorphization under extreme thermal and deformation effects.

The analysis of the structure evolution of the $Ti_{50}Ni_{25}Cu_{25}$ crystalline alloys was carried out in [18] by comparing the force parameters of deformation obtained in the course of the HPT *in situ* with the results of structural studies carried out after the sample was unloaded at different stages of deformation. The aim of the study was to clarify where and how an amorphous phase appears in the case of HPT of crystalline alloys. In work *in situ*, the curve of the change in the torsional moment depending on the deformation value was fixed. Fig. 2 shows the curves for the continuous variation of shear stresses $\sigma(n)$ calculated on the basis of the torsional moment *(M)* data recorded during the deformation at the room temperature of the $Ti_{50}Ni_{25}Cu_{25}$ alloy. The experiments were carried out for an amorphous state obtained by quenching from a melt (curve 2) and for a crystalline alloy obtained by preliminary annealing of the initial amorphous state (curve 1). For comparison, curve 3 is shown in the same figure, corresponding to a change in the shear stress $\sigma(n)$ for polycrystalline copper that does not undergo phase transformations during the HPT process.

Curve 1 can be divided into 3 stages for convenience of further discussion: *I stage* - $0 < n < 2$, at which the level of shear stresses in the material changes insignificantly, and the fraction of the amorphous phase increases to ~ 0.9; *II stage* - $2 < n < 4$, at which the level of shear stresses sharply increases from 350 to 574 MPa. Moreover, the values of the maximum shear stresses s_{max} for the deformation curve 1 for $n \geq 4$ and for curve 2 (points A and A‘, respectively) completely coincide. Then, in *III stage* ($n \geq 4$) HPT, $\sigma(n)$ smoothly decreases from 574 MPa to 450 MPa. Thus, in the view of the force, when $n \geq 4$ the deformation-induced amorphized alloy and the initially amorphous alloy are comparable and behave similarly during further HPT.

The values of the volume fraction of the crystalline phase *V* in the initially crystalline $Ti_{50}Ni_{25}Cu_{25}$ alloy calculated from X-ray and electron microscopic data after different values of the HPT performed at different temperatures (298, 195, and 77K) are shown in Fig. 3. Comparison of the data presented in Fig. 2 and 3 shows that the initial crystalline alloy is almost completely amorphized at room temperature in the interval $0 < n < 4$. Therefore, further

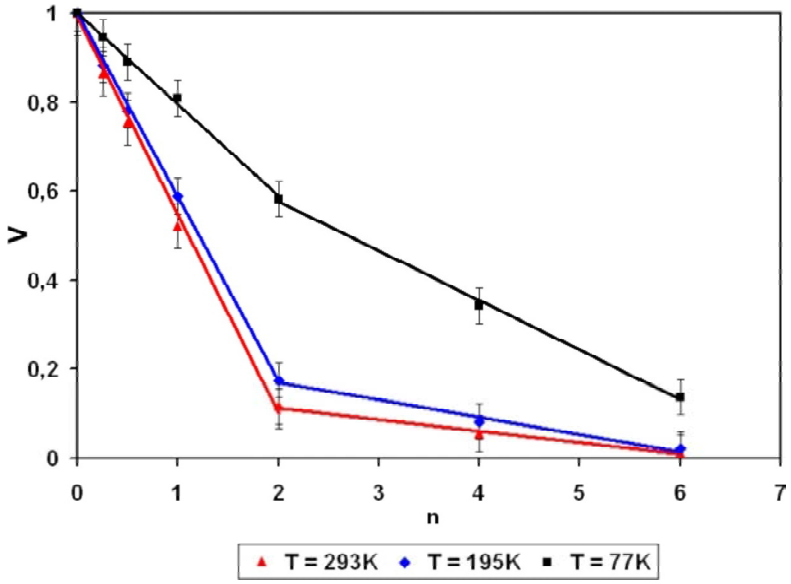

Fig. 3. Dependences of *V(n)* after the HPT of the crystalline $Ti_{50}Ni_{25}Cu_{25}$ alloy at different temperatures.

(in *III stage*), the SPD of an almost completely amorphous material is performed. Analogous processes, but with a lower speed, are revealed during HPT at 195K. At 77K, the amorphization process is noticeably slowed down: so, with a deformation of $n = 6$, a considerable amount of the crystalline phase is still observed (Fig. 3).

Fig. 3 demonstrates that the dependence *V(n)* at all temperatures of HPT has a linear character, and at *n* e" 2 at deformation temperatures of 293K and 195K (to a much lesser extent at 77K) there is a noticeable change (slowing) in the rate of amorphization *dV/dn*. Probably this is due to the change in the mechanism of deformation of an amorphous-nanocrystalline alloy from the intragranular to grain-boundary one upon fragmentation of the structure and a decrease in the size of crystalline fragments and grains to 20-30 nm [19,20].

Assuming that the amorphization of crystalline alloys during HPT is a thermally activated process, it is possible to determine the effective activation energy of the deformation-induced amorphization of the $Ti_{50}Ni_{25}Cu_{25}$ crystal alloy by the expression [21]:

$$\lg(V) = -\frac{E_a}{2.303RT} + \ln A, \qquad (1)$$

where V is the volume fraction of the crystalline phase, E_a is the effective activation energy of the process, A is the constant characterizing the process, T is the temperature, and R is the gas constant.

To determine E_a, see Eq. (1), the lg(V) dependence was plotted against the value 1/T (Fig. 4), from which it is possible to determine the value of E_a for different values of the strain n. All the dependences of $\lg(V) = f(1/T)$ in Fig. 4 have a linear character (correlation coefficient ≈ 0.99). Based on the data obtained in Table 2, the values of the effective activation energy of the deformation-induced process of amorphization of the $Ti_{50}Ni_{25}Cu_{25}$ crystal alloy at HPT after various n are presented.

As follows from the table, the effective activation energy for the process of deformation-induced amorphization is very small in absolute value, but it increases smoothly as the strain increases during HPT. However, even at $n = 6$, the value of $(E_a)_{max}$ is only about 0.02 eV, which is much lower than the activation energy of migration of replacement atoms at room temperature, not only by the vacancy mechanism (0.8-1.0 eV), but even by the migration mechanism of interstitial atoms (0.1-0.2 eV) [22].

At the same time, the value of $(E_a)_{max}$ is close enough to the atoms' migration values along the crowdion mechanism (0.02-0.04 eV) [23]. Therefore, along with the small influence of the thermally acti-

Table 2. The values of E_a as a function of n for the $Ti_{50}Ni_{25}Cu_{25}$ alloy.

n	E_a, J/mol	$Å_á$, eV·10^{-4}
1/4	76.6	7.94
1/2	143.6	14.9
1	379.1	39.3
2	1 357.5	141.0
4	1 566.2	162.0
6	2 048.7	212.0

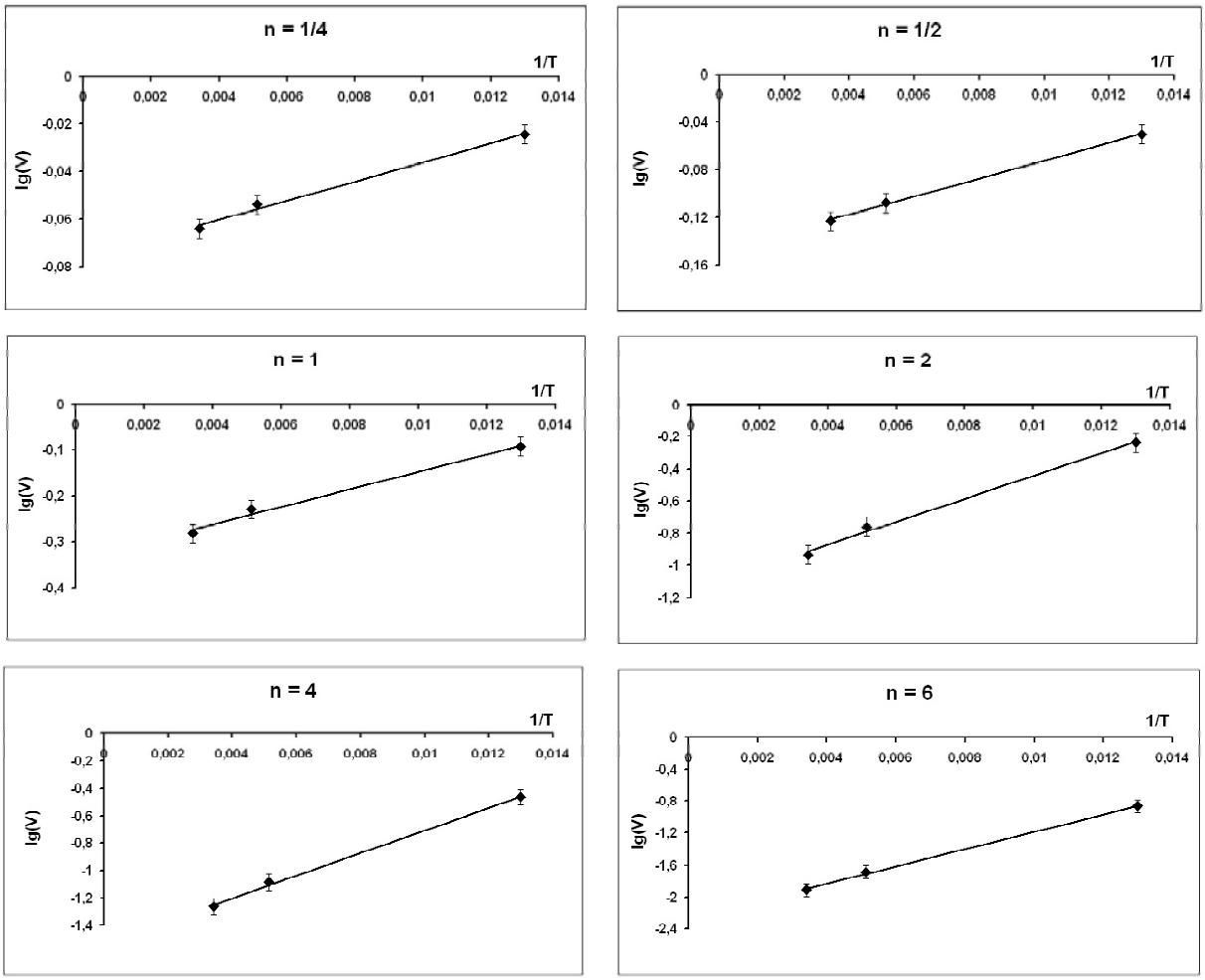

Fig. 4. Dependency graphs in the coordinates lg(V) = f(1/T) after HPT for the crystalline $Ti_{50}Ni_{25}Cu_{25}$ alloy for different values of n.

vated processes responsible for deformation-induced amorphization, a shifting athermal process plays an important role. In this connection it is appropriate to recall the ideas set forth in the works of A.E. Romanov and V.I. Vladimirov [24]. They suggested that, with a high concentration of point defects (vacancies or crowdions), their long-range interaction leads to the appearance of new properties of the ensemble of point defects. In particular, they can form flat discs equivalent to dislocation loops. The collective motion of these defects is capable of performing a quasi-dislocation plastic shear in the form of an avalanche-like displacement of point defects. Such a process obviously has low activation energy and can be considered as the basis for the transition of a defective crystal to an amorphous state at SPD.

At the structural level, electron microscope studies of the $Ti_{50}Ni_{25}Cu_{25}$ alloy after HPT at 293K showed that the average grain size of the crystalline phase decreases from 500-2000 nm in the initial state to ~ 4-5 nm in the second stage of deformation $n \geq 2$ [18]. In case of extreme deformation, in particular during the shear under pressure, it is noted that the minimum size of nanocrystals can reach 10 nm [25]. However, with an average grain size ≤10-20 nm, the probability of existence of developed dislocation modes is small [26]. The theoretical possibility of a cardinal change in the deformation mechanism from inter-grain to grain-boundary one with a grain size ≤20, was first shown in [27, 28]. The key element of the structure, which determines the flow of plastic deformation of nanocrystalline materials with such a small size of crystallites, becomes grain boundaries. As shown by experiments, low-temperature grain-boundary slip and associated with it, grain displacements relative to each other as well as their mutual rotations, are activated in the structure. Proceeding from the condition of preservation of the continuity of the material, this process must be accompanied by the emission of deformation vacancies from triple junctions and steps at the grain

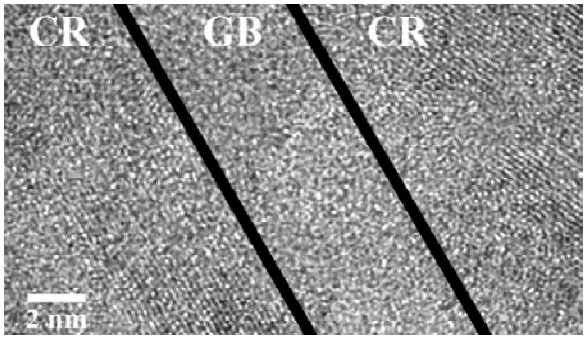

Fig. 5. Electron microscopic image of $Ti_{50}Ni_{25}Cu_{25}$ alloy structure in direct mode after HPT (n = 1/2); CR - crystalline phase; GB is the grain boundary region in the amorphous state.

boundaries into the body of the grain. The grain boundaries, which are not only sources but also sinks of defects, absorb vacancies, storing excess non-equilibrium free volume, and are partially amorphous (Fig. 5). Further deformation leads to a repetition of the process many times. Vacancies flow through the volume of grain and are absorbed in the compressed areas of the boundary, as a result of which the boundaries expand [18].

It is known that for small grain sizes, most of the atoms are located within the boundaries [29]. Based on these considerations, and based on the experimental data obtained, we may assume that at the initial stage of amorphization the structure of the material becomes biphasic - a “grain boundary frame” is formed from amorphous layers (Fig. 6), in cells of which there is a defective nanocrystalline phase with a high concentration lattice defects and clusters of the vacancy nature. One of the possible mechanisms of athermal amorphization in this case could be the cooperative shear mechanism resulting from the long-range interaction of crowdions.

During HPT, the thickness of the “grain-bound framework” increases. It is transformed into a massive amorphous phase, which occupies the increasing volume. Under conditions of suppression of the processes of dynamic recrystallization, the concentration of point defects (vacancies, interstitial atoms or crowdions) in certain regions of grain boundaries may exceed the critical value C_{cr}, leading to a loss of stability of the crystal. The value of C_{cr} can be estimated us

$$C_{cr} = \Delta H_{vak} / \Delta H_f \approx 0.08, \quad (2)$$

where ΔH_{vak} and ΔH_f are the specific heat of formation and melting of point defects, respectively.

As a result, the effective rate of grain-boundary diffusion sharply increases, the instability of the crystalline phase, leading to a loss of translational symmetry and to phase transition of a crystalline phase to the amorphous one, develops.

The possibility of boundary transition to an amorphous state during SPD has also been shown in a number of papers on the molecular dynamics modeling [31-33]. The experimental data correlate with the presented theoretical work and the general assumptions about the existence of an amorphous “grain-boundary framework”, expanding during deformation, are to some extent justified.

3. DEFORMATION-INDUCED CRYSTALLIZATION.

On the basis of the above, amorphous alloys obtained, for example, by quenching from a melt, must remain amorphous when subjected to SPD. However, as it was found [10,34,35], that during SPD, nanocrystallization of an amorphous phase occurs: homogeneously or heterogeneously located nanocrystals about 10-20 nm in size are observed in the amorphous matrix.

The appearance of nanocrystals homogeneously distributed throughout the volume of the amorphous matrix at room temperature is difficult to explain within the framework of the classical concepts of the thermally activated nature of crystallization processes. An attempt was made in [36,37] to analyze in detail the features of the structure and properties

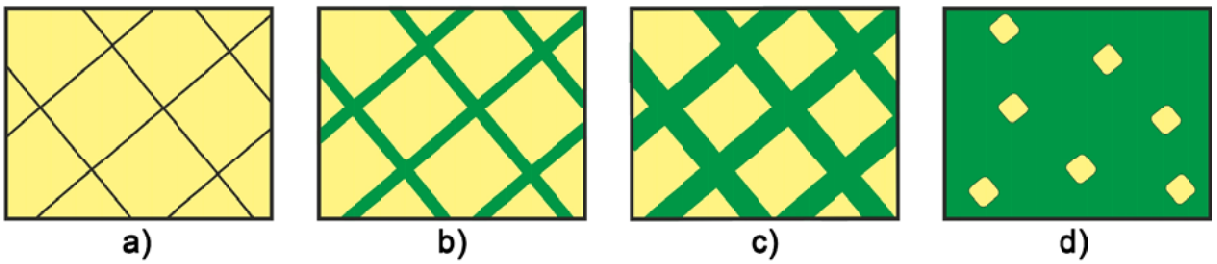

Fig. 6. Scheme of structural transformations during the transition “crystal-amorphous state” with SPD: a) fragmentation of the structure; b) formation of boundaries with an amorphous structure; c) increase in the specific volume of grain-boundary amorphous layers; d) amorphous-nanocrystalline state.

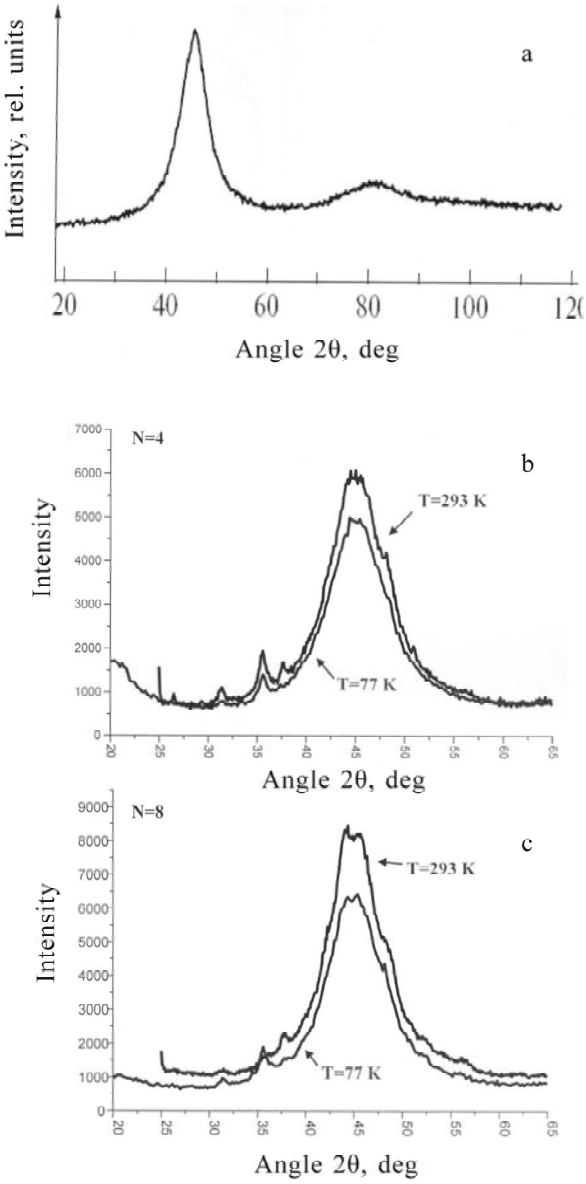

Fig. 7. X-ray diffraction diagrams of the $Ni_{44}Fe_{29}Co_{15}Si_2B_{10}$ amorphous alloy in the initial condition after melt quenching (a), after n = 4 at 293K and 77K (b) and after n = 8 at the same deformation temperature (c).

under the influence of SPD on a number of amorphous metal-metalloid-type alloys produced by quenching from a melt ($Ni_{44}Fe_{29}Co_{15}Si_2B_{10}$, $Fe_{74}Si_{13}B_9Nb_3Cu_1$ (Finemet), $Fe_{57,5}Ni_{25}B_{17,5}$, $Fe_{49,5}Ni_{33}B_{17,5}$, $Fe_{70}Cr_{15}B_{15}$), and $Ti_{50}Ni_{25}Cu_{25}$. Fig. 7 shows the X-ray diffraction patterns of the amorphous Ni-Fe-Co-Si-B alloy in the initial state (a), after n = 4 at 293K and 77K (b) and after n = 8 for the same deformation temperatures (c). It can be seen that, after HPT, the crystallization processes in the alloy have started, expressed more noticeably after deformation at room temperature. The special computer program allowed determining the volume fraction and the size of the crystalline phase in the case of the X-ray diffraction patterns shown in Fig. 7. For example, for n = 4 and T = 293K, the fraction of crystalline phase V and the average crystallite size d are 8% and 3 nm, respectively. It is worth to note that the values of these parameters correspond almost completely to those observed after n = 8, but at T = 77K (V = 6% and d = 2 nm). Electron microscopic observations confirmed these results qualitatively and quantitatively.

For $n \leq 2$, non-homogeneous plastic deformation is observed in the $Ni_{44}Fe_{29}Co_{15}Si_2B_{10}$ alloy with formation of coarse shear bands, which is typical to the deformation of all amorphous alloys at temperatures considerably below the transition point to the crystalline state [38]. Local shear bands can be observed by transmission electron microscopy on samples after deformation due to crystallization effects (Fig. 8). Otherwise, the contrast on the electron microscope image can only be of an absorption nature and does not arise after preliminary operations for preparing thin foils for electron microscopic analysis. The theoretical estimates show that the local and short-term (not more than a few microseconds) temperature increase in the shear bands can reach 500 °C [39]. In this case, the local temperature in the zone of plastic shear may exceed the crystallization temperature of the amorphous alloy (in our case T_{cr} = 410 °C) and lead to the formation of a primary fcc-phase in the shear bands. This is confirmed by the results in Ref. [37], where it is shown that the higher the crystallization temperature of an amorphous alloy, the smaller is the volume fraction of the crystalline phase formed during the HPT process at room temperature (Fig. 9). To date, much evidence has been accumulated

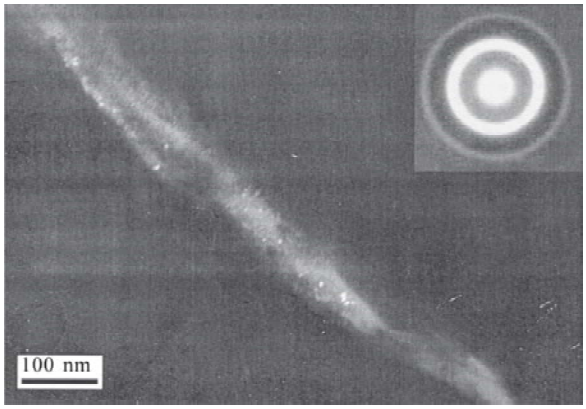

Fig. 8. Electron microscopic image of the crystallized local shear band in the $Ni_{44}Fe_{29}Co_{15}Si_2B_{10}$ amorphous alloys after severe plastic deformation (n = 0.5; T= 293K).

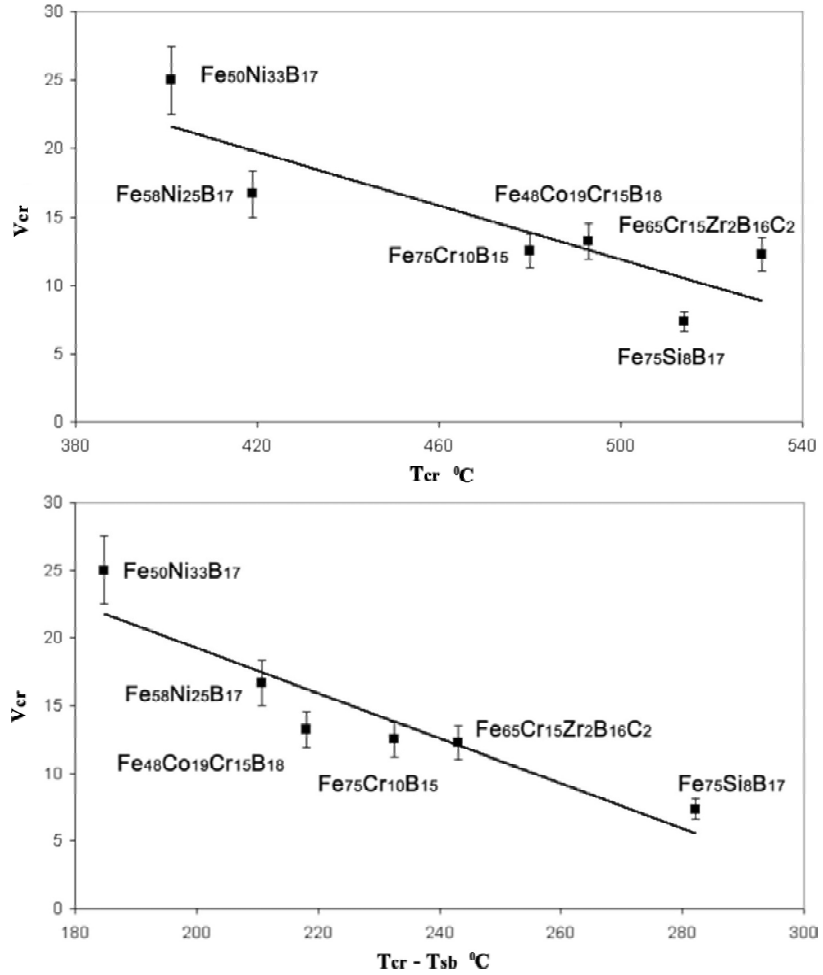

Fig. 9. Correlation between the values of V and T_{cr} for the amorphous alloys without taking into account (a) and taking into account (b) different dissipative capacity of the shear bands; correlation coefficient $r = 0.74$ (a) and $r = 0.86$ (b).

that a noticeable local temperature increase is observed in the shear bands. First of all, we should mention the witty experiment of J.J. Lewandowski and A.L. Greer [40], with the deposition of a low-melting material on the surface of a sample of an amorphous alloy before deformation, as well as direct experiments on recording the temperature in the shear band in a massive amorphous alloy [41]. In addition, as a result of local and short-term temperature increases, a special character of the electron microscopic contrast in an amorphous structure and a change in the values of nanosurfaces in the immediate vicinity of the location of the shear band in amorphous alloys have recently been observed [42,43]. It is also impossible to exclude some influence on the processes of crystallization of an increased concentration in the shear bands of regions of excess free volume, which was first recorded in Ref. [44]. It was also established [38] that the topological short-range order typical to amorphous alloys, obtained by quenching from the melt, is violated in the shear bands.

At later stages of HPT of amorphous alloys ($n \geq 2$), the deformation pattern changes drastically [45]. Shear bands are practically not observed. Instead, it is possible to reveal in the structure nanoparticles of the crystalline phase up to 10 nm in size, homogeneously located throughout the sample volume (Fig. 10). Consequently, the process of plastic deformation of amorphous alloys changes from strongly a localized and inhomogeneous to the "quasi-homogeneous" one. As is known, such a nature of plastic flow is inherent in amorphous alloys at very high temperatures close to the glass transition point under the conditions of a sharp decrease in the dynamic viscosity of metallic glass [38]. In this case, to achieve such a "softened" state at room temperature, and moreover at 77K, is hardly possible. Apparently, we are dealing with the manifestation of a fundamentally new structural mecha-

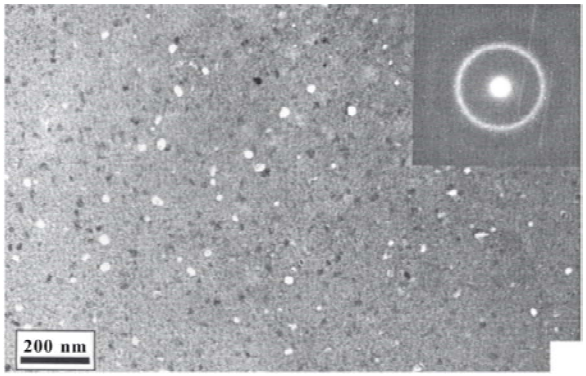

Fig. 10. Dark field image of the $Ni_{44}Fe_{29}Co_{15}Si_2B_{10}$ amorphous alloy after n = 8 at 77K.

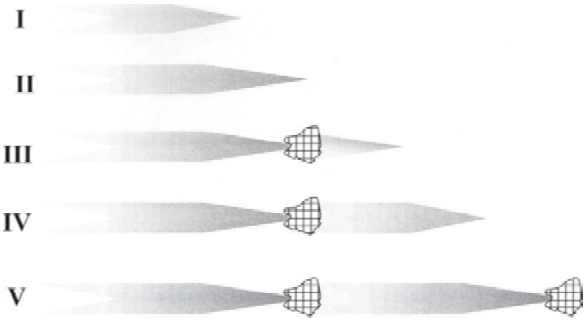

Fig. 11. The mechanism of "self-blocking" of shear bands propagating in the amorphous matrix.

nism of plastic deformation of amorphous alloys, which occurs only under SPD conditions.

One possible explanation of the observed delocalization of plastic flow is as follows [45]. As the shear band propagates in the amorphous matrix during the HPT process, its temperature constantly rises, while at the propagation front of the band it is always maximum (*I* in Fig. 11). There comes such a moment when the local temperature on the front of the shear band reaches the crystallization temperature. (*II* in Fig. 11), and as a consequence, a nanocrystal appears on the front of the growing band, which sharply inhibits the plastic flow zone, since the resulting crystal has nanoscale dimensions and is incapable of dislocation plastic flow. There are two options for further developments. First, under the action of the shear band, the nanocrystal will accumulate a high level of elastic stresses, as a result of which a new shear band will emerge in the amorphous matrix according to the mechanism of elastic accommodation (*III* in Fig 11). In this case, the process of plastic flow will pass through the relay mechanism, generating in the shear band the formation of nanocrystals equidistantly located along the trajectory of motion of the shear band in the amorphous matrix. This is confirmed by the electron microscopic image in Fig. 12, where the chains of such equidistantly located nanocrystals are actually visible. Secondly, the branching of shear bands, which are inhibited due to frontal formation of nanocrystals, is possible. This process, somewhat reminiscent of the multiplication of dislocations on noninterruptible particles, is schematically shown in Fig. 13. As a result of this "self-inhibition" of the shear bands on the frontal nanocrystals, the inhomogeneous plastic flow is delocalized. The essentially observed effect of the transition to homogeneous nanocrystallization on shear bands means that the plastic flow is characterized by a high bulk density of shear bands and, as a consequence, a homogeneous character of the nanocrystal precipitation in more "thin" shear bands. Recently, a similar

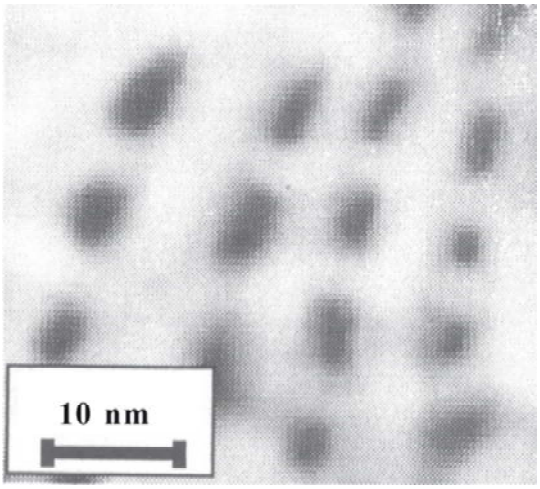

Fig. 12. The chains of equidistant nanocrystals, formed in severe plastic deformation of the Fe-Ni-B amorphous alloy. Transmission electron microscopy.

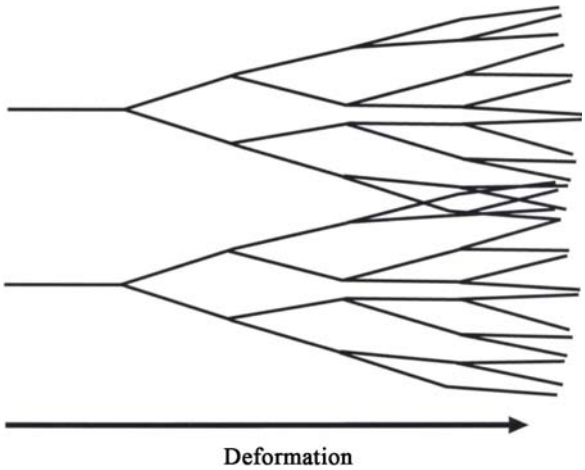

Fig. 13. The mechanism of multiplication of the shear bands as a result of interacting with the frontal nanocrystals.

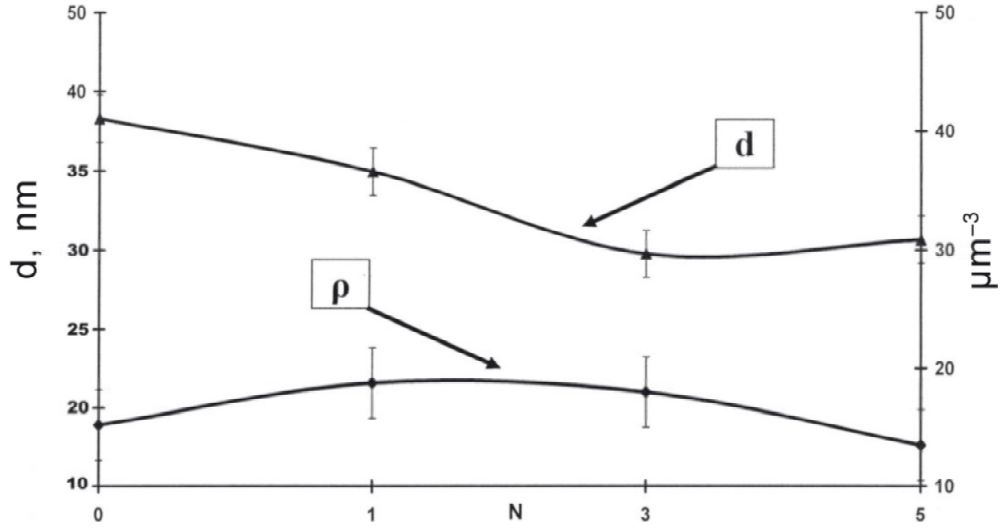

Fig. 14. Dependence of the average size (*d*) and volume density (ρ) of the nanoparticles of the crystalline phase in the initial partially crystallized alloy $Ni_{44}Fe_{29}Co_{15}Si_2B_{10}$ on the value of *n* in severe plastic deformation (*T* = 293K).

effect of delocalization of plastic flow was observed in a massive amorphous alloy based on Zr [46].

Let us turn to the general energy concept of SPD [47]. In the process of deformation, we introduce a considerable elastic energy into the solid. As possible channels of dissipation in this case it is necessary to analyze plastic deformation, phase transformations and heat release. The cause of crystallization is both the local increase in temperature, and the presence of significant local stresses in the amorphous matrix. Stresses stimulate the flow of processes that depend on the temperature, and the higher the voltage, the lower the temperature of the flow of thermally activated crystallization processes. In addition, we must take into account the fact that the value of the activation energy of the crystallization process ***Q**** is lower than usual due to a higher concentration in the shear bands of regions of excess free volume [44]. Finally, one more important detail must be taken into account: the local atomic structure of the amorphous matrix in the shear band can differ from the "classical" one for the amorphous state [38]. It is quite possible that in the amorphous matrix even before crystallization there are regions induced by deformation with increased correlation in the arrangement of atoms - the nuclei of the crystalline phase with a markedly different degree of compositional and topological short-range order. This is indirectly evidenced by the results in Ref. [48], which shows that the chemical composition of the crystalline phase in an amorphous aluminum-based alloy after conventional annealing and after HPT is significantly different.

In this way,

$$Q^* = Q_k - G\tau - \Delta Q_{co} - \Delta Q_{bn}, \quad (3)$$

where Q^* is the effective activation energy of crystallization in the shear band, Q_k is the activation energy of crystallization due to thermal fluctuations, *G* is the shear modulus, and *t* is the shear stress in the region of the plastic shear zone. $\Delta Q_{áí}$ - a contribution to the decrease in activation energy of crystallization due to the presence of short-range order (topological and/or composite) in the zone of the shear band and $\Delta Q_{ñí}$ - a contribution to the decrease in activation energy of crystallization due to substantial enrichment of the shear band by excess free volume.

In [49] another interesting phenomenon, typical to SPD amorphous alloys, was discovered. By lowering the HPT temperature to 77K, it was possible to suppress the manifestation of crystallization effects in amorphous Fe-Ni-B alloys. In this case, the EXAFS method using synchrotron radiation, made it possible to reveal that HPT at 77K destroys the short-range compositional and topological short-range order in the arrangement of atoms and compacts the amorphous matrix, increasing the average coordination number and reducing the average radius between pairs of atoms of different types in the first coordination sphere of iron atoms. In other words, the structure of the alloys after this treatment becomes perfectly amorphous, which is confirmed by the results of calorimetric analysis. Probably, under these deformation conditions an in-

creased plasticity of amorphous materials will be observed.

4. CYCLICITY OF PHASE TRANSFORMATIONS

The study of the SPD of partially crystallized Fe, Ni, and Co based alloys led to unexpected results [50]. The partially crystalline state formed after annealing of an amorphous alloy becomes amorphous again as the strain increases to $n = 5$. Electron microscopic experiments unequivocally confirmed this trend: a sharp decrease in the size of nanocrystals occurs while their bulk density remains. Such an unusual evolution of an amorphous-nanocrystalline structure with increasing ***n*** is clearly demonstrated by the dependence of an average size of nanoparticles and their bulk density with increasing *n* in a partially crystallized amorphous alloy (Fig. 14). With practically unchanged amount of nanoparticles per unit volume, the disappearance of a crystalline phase occurs due to a significant decrease in the size of nanoparticles, in other words, due to their "dissolution" in an amorphous matrix.

It should be noted that the appearance of crystals in amorphous shear bands occurs in the SPD process, and not after its completion. Therefore, the shear bands newly arising in the amorphous matrix begin to interact with the nanocrystallites formed at the earlier SPD stages. Such an interaction can occur through several mechanisms [51]: inhibition of shear bands on the particles of the crystalline phase, cutting or shearing around such particles, and the effects of primary and secondary accommodation. In any case, such an interaction will cause the appearance of dislocations in the crystalline particle itself. The highest dislocation density will, obviously, be near the interphase boundary, where the effect of shear bands will be most effective. Finally, there comes a time when the density of dislocations in the border zone will be extremely high, and it (or the entire crystalline particle) will spontaneously transfer into the amorphous state in accordance with the reasons stated in Section 2. In reality this will be perceived as the "dissolution" of crystals under action actively acting in an amorphous matrix of shear bands during SPD. Exactly that process of "dissolution" was observed during SPD of a partially crystallized amorphous alloy [50]. It should be kept in mind that the deformation "dissolution" of crystals is unlikely to be fulfilled completely. It is known [26] that very small crystalline particles (less than 10 nm) can not accumulate dislocation-type defects due to the presence of very large image forces. In our case, this means that nanocrystalline particles smaller than 10 nm in the amorphous matrix will not "dissolve" during the SPD process. They are structurally stable and will persist throughout the long stages of SPD. Therefore, it is easy to explain the fact that in all studies without exception, where the crystal precipitation process was recorded during SPD, they always had sizes less than 20 nm [3].

At the same time, as the experiment shows, there are cases where the balance between the release of crystals on the shear bands and the subsequent deformation "dissolution" can be violated. In this case, the principle of cyclicity is triggered at the SPD, and structural states with large and small volume fractions of nanocrystals in the amorphous matrix periodically replace one another as the strain increases. Earlier, a similar effect was observed in the course of experiments on mechanoactivation of Co_3Ti intermetallide powder [52]. Such a cyclicity, that is, a tendency to a phase transition of the initially amorphous structure to the crystalline state, and vice versa, the existence of the directly opposite trend at certain stages of SPD in a consistent manner explains, in our view, the apparent contradiction in the experimental results of a number of studies [3].

It is of undoubted interest to analyze the features of cyclic deformation-induced amorphization and crystallization for the same material with varying its initial state, which would allow creating the single structural model of cyclic phase transformations in the HPT process. In the initially amorphous $Ti_{50}Ni_{25}Cu_{25}$ alloy, as in the initially crystalline alloy of the same composition, in the course of increasing strains, the following cyclic sequence of phase transitions is observed [53]:

$$B19 \Rightarrow AF \Rightarrow B2 \Rightarrow B19 \Rightarrow AF \Rightarrow B2, \qquad (4)$$

where AF is the amorphous state of a solid.

The frequency of structural changes during SPD is generally determined by the activation of various elastic energy dissipation channels stored by the material during deformation [47]. It is obvious that the features of the structural change in the $Ti_{50}Ni_{25}Cu_{25}$ alloy during SPD observed in Ref. [53] are related to the peculiarities of the flow of direct and inverse phase transformations of both diffusion and martensitic type. Expression (4) is a diagram giving an idea of the nature of cyclic transitions at SPD from the crystalline state to the amorphous one and then from the amorphous to the nanocrystalline one with subsequent periodic repetition of processes but already at the nanoscale

level. It is interesting to note that an amorphous state in the SPD process is formed only upon deformation of the crystalline B19 phase, and with further deformation of the amorphous state, the crystal phase B2 always appears.

5. CONCLUSIONS

Thus, we come to the conclusion that, both during deformation of intermetallic compounds and complex phases prone to amorphization at SPD, and during deformation of initially amorphous alloys, the SPD undergoes successive transitions from the amorphous state to the crystalline one, and vice versa, from the crystalline to the amorphous one. As a result, a stable amorphous-nanocrystalline structure is formed, undergoing quantitative changes as the strain continues to grow. Stable amorphous-nanocrystalline structures arising at significant SPD are essentially a stationary state in accordance with the basic principles of nonequilibrium thermodynamics, which can correctly describe the processes occurring during large plastic deformations [6,47].

ACKNOWLEDGEMENT

The work was supported by State Task no. 2017/113 of Ministry of Education and Science of the Russian Federation as well as by the Russian Foundation for Basic Research, project no. 18-02-00805_à. The author (RVS) are very grateful to Russian Science Foundation project no. 18-72-00026 for help in TEM analysis.

REFERENCES

[1] A.Vinogradov and Yu. Estrin // *Progr. Mater. Sci*. **95** (2018) 172.
[2] K. Edalati and Z. Horita // *Mater. Sci. Engi*n. **A 652** (2016) 325.
[3] A.M. Glezer, E.V. Kozlov, N.A. Koneva, N.A. Popova and I.A. Kurzina, *Plastic Deformation of Nanostructured Materials* (CISP- Taylor & Francis Group, New-York, 2017).
[4] Zs. Kovacs, P.Henits, A.P. Zhilyaev and A. Revesz // *Scr. Mater*. **54** (2006) 1733.
[5] A.V. Sergueeva, C. Song, R.Z. Valiev and A.K. Mykherjee // *Mater. Sci. Engin. **A*** **339** (2003) 159.
[6] L.S. Metlov // *Phys. Rev.* **E 81** (2010) 051121.
[7] A.P. Zhilyaev and T.L. Langdon // *Progr. Mater. Sci*. **53** (2008) 893.
[8] A.M. Glezer, L.S. Metlov, R.V. Sundeev and A.V. Shalimova // *JETP Letters* **105** (2017) 332.
[9] H. Nakayma, K.K. Tsuchiya and M. Umemoto // *Scr. Mater.* **44** (2001) 1781.
[10] J.Y. Huang, Y.T. Zhu, X.Z. Liao and R.Z. Valiev // *Phil. Mag. Lett.* **84** (2004) 183.
[11] R.V. Sundeev, A.V. Shalimova, A.A. Veligzhanin, A.M. Glezer and Y.V. Zubavichus // *Mater. Lett.* **214** (2018) 115.
[12] Y.V. Tatyanin and V.G. Kurdjumov // *Phys. Stat. Sol. (a)*. **121** (1990) 455.
[13] K. Inaekyan, V. Brailovski, S. Prokoshkin, A. Korotitskiy and A. Glezer // *J. Alloys and Comp.* **473** (2009) 71.
[14] V.I. Zeldovich, N.Yu. Frolova, V.P. Pilyugin, V.M. Gundyrev and A.M. Patselov // *Phys. Met. Metallogr.* **99** (2005) 425.
[15]. V. Brailovski, S.D. Prokoshkin, I.Y. Khmelevskaya, K.E. Inaekyan, V. Demers, S.V. Dobatkin S.V and E.V. Tatyanin // *Mater. Trans. JIM.* **47** (2006) 795.
[16] R.V. Sundeev, A.M. Glezer and A.V. Shalimova // *J. Alloys and Comp.* **611** (2014) 292.
[17] R.V, Sundeev, A.M. Glezer and A.V. Shalimova // *Mater. Lett.* **175** (2016) 72.
[18] R.V. Sundeev, A.V. Shalimova, A.M. Glezer, E.A. Pechina, M.V. Gorshenkov and G.I. Nosova // *Mater. Sci. Engin. **A*** **679** (2017) 1.
[19] A.M. Glezer and A.A. Tomchuk // *Rev. Adv. Mater. Sci.* **45** (2016) 246.
[20] V.G. Gryaznov and L.I. Trusov // *Progr. Mater. Sci. **3**7* (1993) 289.
[21] C. Zhang, J.C. Qiao, J.M. Pelletier and Y. Yao // *Intermetallics* **86** (2017) 88.
[22] V.V. Sagaradze, V.A. Shabashov, N.V. Kataeva, V.A. Zavalishin, K.A. Kozlov, A.R. Kuznetsov, A.V. Litvinov and V.P. Pilyugin // *Phil. Mag.* **96(17)** (2016) 1724
[23] P.M. Derlet, D. Nguyen-Manh and S.L. Dudarev // *Phys. Rev. B* **76** (2007) 054107.
[24] A.E. Romanov and V.I. Vladimirov, In: *Dislocations and Disclinations*, ed. by F.N.R. Nabarro (Belsevier, Amsterdam-Tokyo, 1992) **9** 191.
[25]. A. V. Korznikov, A.N. Tyumentsev and I.A. Ditenberg // *Phys. Met. Metallogr.* **106** (2008) 418.
[26] V.G. Gryaznov, A.M. Kaprelov and A.E. Romanov // *Scr. Metal.* **23** (1989) 1443.
[27] A. M. Glezer and V.A. Pozdnyakov // *Nanostr. Mater.* **6** (1995) 767.
[28] M.A. Meyers, A. Mishra and D.J. Benson // *Progr. Mater. Sci.* **51** (2006) 427.

[29] R.A. Andrievski and A.M. Glezer // *Physics-Uspekhi* **52** (2009) 315.
[30] W.L. Johnson // *Progr. Mater. Sci.* **30** (1986) 81.
[31] H. Van Swygenhoven and A. Caro // *Phys. Rev*. **B 58** (1998) 246.
[32] H.N. Jarmakani, E.M. Bringa, P. Erhart, B.A. Remington, Y.M. Wang, N.Q. Voc and M.A. Meyers // *Acta Mater*. **56** (2008) 5584.
[33] A.M. Glezer,V.L. Stolyarov, A.A. Tomchuk and N.A. Shurygina // T*echn. Phys. Lett.* **42** (2016) 51.
[34]. H. Chen, Y. He, G.J. Shiflet and S.J. Poon // *Lett. Nature.* **367** (1994) 541.
[35] A.M. Glezer, S.V Dobatkin, M.R Plotnikova and A.V Shalimova // *Mater. Sci. Forum*. **584-586** (2008) 227.
[36] A.M. Glezer, M.R. Plotnikova, A.V. Shalimova and S.V. Dobatkin // *Bull. Russ. Acad. Sci. Phys.* **73** (2009) 1302.
[37] P.V. Sundeev, A.M. Glezer, A.V. Shalimova, N.V. Umnova and G.I. Nosova // *Russ. Metall. (Met.)* **10** (2014) 778.
[38] A.M. Glezer, A.I. Potekaev and A.O. Cheretaeva, T*hermal and Time Stability of Amorphous Alloys* (CISP- Taylor & Francis Group, New-York, 2017).
[39] A.M. Glezer, S.G. Zaichenko and M.R. Plotnikova // *Bull. Russ. Acad. Sci. Phys.* **76** (2012) 54.
[40] J.J. Lewandowski and A.L. Greer // *Nature Mater.* **5** (2006) 15.
[41] A.I. Bazlov, A.Yu Churyumov, S.V. Ketov and D.V. Louzguine-Luzgin // *J. Alloys Comp*. **619** (2015) 509.
[42] J. Pan, Q. Chen, L. Liu and Y. Li // *Acta Mater*. **59** (2011) 5146.
[43] R. Maaâ, K.Samwer, W. Arnold and C.F. Volkert // *Appl. Phys. Lett.* **105** (2014) 171902.
[44] P.E. Donovan and W.M. Stobbs // *Acta Met.* **29** (1981) 1419.
[45] A.M. Glezer, M.R. Plotnikova, R.V. Sundeev and N.A. Shurygina // *Bull. Russ. Acad. Sci. Phys*. **77** (2013) 1391.
[46] E.V. Ubyivovk, E.V. Boltynjuk, D.V. Gunderov, A.A. Churakova, A.R. Kilmametov and R.Z. Valiev // *Mater. Lett.* **209** (2017) 327.
[47] A.M. Glezer and R.V. Sundeev // *Mater. Lett.* **139** (2015) 455.
[48] A. Aronin, D. Matveev, E. Pershina, V. Tkatch and G. Abrosimova // *J. Alloys Comp*. **715** (2017) 176.
[49] R.V. Sundeev, A.M. Glezer, A.P. Menushenkov, A.V. Shalimova, O.V. Chernyshova and N.V. Umnova // *Mater. Design* **135** (2017) 77.
[50] A.M. Glezer and I.E. Permyakova, *Melt-Quenched Nanocrystals* (CISP- Taylor & Francis Group, New-York, 2013).
[51] A.M. Glezer, N.A. Shurygina, S.G. Zaichenko and I.E. Permyakova // *Russ. Metall. (Met.*) **4** (2013) 235.
[52] M. Sherif - Eskandarany, K. Aoki, K.Sumiyama and K. Suzuki // *Acta Met.* **50** (2002) 1113.
[53] R.V. Sundeev, A.M. Glezer and A.V. Shalimova // *Mater. Lett.* **133** (2014) 32.